

Analyzing the causes for the dispersion of the fast reactor spent fuel rod cladding properties*

Valeriy N. Shemyakin¹, Evgeniy A. Kinev¹, Aleksander V. Kozlov¹, Irina A. Portnykh¹, Valeriy L. Panchenko¹, Mikhail V. Evseev¹

¹ Research Institute of Nuclear Materials, POB 29, Zarechny, Sverdlovsk Reg., 624250, Russia

Corresponding author: Evgeniy A. Kinev (kinev007@yandex.ru)

Academic editor: Yury Korovin ♦ Received 12 August 2019 ♦ Accepted 21 October 2019 ♦ Published 10 December 2019

Citation: Shemyakin VN, Kinev EA, Kozlov AV, Portnykh IA, Panchenko VL, Evseev MV (2019) Analyzing the causes for the dispersion of the fast reactor spent fuel rod cladding properties. Nuclear Energy and Technology 5(4): 323–329. <https://doi.org/10.3897/nucet.5.48423>

Abstract

The swelling, corrosion and high-temperature embrittlement behavior of the fast-neutron sodium-cooled reactor standard and test fuel rod claddings was studied following the operation up to a damaging dose of 55 to 69 dpa. The tested characteristics were found to differ sensitively in conditions similar to irradiation for the claddings of the experimental tube conversion technology. Unlike the standard fuel rod claddings, the test rod claddings were additionally heated in the process of fabrication to homogenize the solid solution at different temperatures and austenitization times. On the whole, this led to an increased cladding resistance contrary the damaging factor of the reactor environment. The positive effect is explained by the influence of carbon and the morphology of swelling-reducing alloying elements, as well as by the nature of the carbide and intermetallic phase precipitation. However, the dispersion of the post-irradiation properties which remained significant and was also earlier observed in the standard rods is explained by potential differences in the heat treatment technology and the irradiation temperature in conditions of a hard-to-control coolant flow velocity. The swelling rate and the in-fuel corrosion depth for the test technology tubes were respectively 0.04 to 0.058%/dpa and 20 to 47 μm ; similar values for the test material are 0.036 to 0.056%/dpa and 15 to 35 μm respectively. The short-term mechanical properties of the test fuel rods at a temperature of 600 °C showed a smaller tendency towards high-temperature embrittlement. The dispersion of the properties was caused by the chemical and structural heterogeneity as the result of the tube fabrication.

Keywords

Fuel rod, cladding, swelling rate, corrosion, grain size, high-temperature embrittlement, manufacturing technology.

1. Introduction

Examinations of spent fuel assemblies often show different amounts of the cladding diameter change in seemingly identical fuel rods manufactured, using one and the same technology, from the metal of the same heat and

with the experience of service in very close temperature and dose conditions (Bakanov et al. 2011, 2011a). Further material studies identify an equally considerable difference in the cladding properties such as magnitude of swelling (Portnykh et al. 2007), degree of the inner surface corrosive damage, and strength and ductility at elevated

* Russian text published: Izvestiya vuzov. Yadernaya Energetika (ISSN 0204-3327), 2019, n. 3, pp. 96–107.

temperatures (Barsanova et al. 2018). The dispersion of properties can be supposedly caused by the chemical (segregational) heterogeneity of the metal or by its structural heterogeneity as the result of the tube fabrication process (Bakanov et al. 2005; Tselishchev et al. 2010). The condition of a test assembly with the fuel cladding manufactured using three different technologies has been studied to check these statements.

2. Materials and procedures

The study was conducted for fuel rods from the 06Cr-16Ni15Mo2MnTiPB steel of two meltings having chemical compositions meeting Specs 14-131-960-2001 (Spitsyn et al. 2015) but being relatively different in the content of elements the most significant of which are B, N, P, S, and Si (Table 1).

The tube conversion for all of the claddings was based on a multi-stage technology (Tselishchev et al. 2010; Spitsyn et al. 2015) which is currently in the process of adjustment. The experimental cladding fabrication technology differed from the standard technology in a longer (approximately fivefold) hold time during recrystallization annealing at the same temperature. At the finished fuel rod stage, the cladding was heated to 500 ± 50 °C in the process of a leak-tightness test with a hold time of not more than five hours (Bakanov et al. 2005).

The additional test cladding mode included annealing in the middle of the tube conversion process (intermediate billet diameter) with one of the tube batches annealed at 1180 °C for three hours and the other tube annealed at 1060 °C for 20 minutes.

The test assembly was composed of statistically credible number of fuel rods (Melt B) manufactured using a technology with an additional heat-up to 1060 °C and claddings of the same heat manufactured with an additional heat-up to 1180 °C. Across the fuel assembly, the test rods were uniformly distributed among the standard assemblies with the Melt A claddings. The assembly operated in the BN-600 reactor core up to a damaging dose of about 70 dpa. Following the assembly dismantling, the maximum relative diameter changes were recorded for all

of the test and standard claddings (Table 2). The diameter of the cladding in the fuel rod's lower gas space zone, where no diameter changed due to irradiation, was assumed to be the initial cladding diameter.

Five of the fuel assembly's rods were examined at JSC INM. Material studies were conducted on fuel rods No. 1 (from the assembly's peripheral row being the nearest to the core center) and No. 2 (from the assembly's center) with the Melt A claddings manufactured using the standard technology (the greatest and the smallest possible diameter change), fuel rod No. 3 (from the assembly's center, contacting fuel rod 2) with the Melt B cladding manufactured with a heat-up to 1060 °C (the smallest diameter change), and fuel rods No. 4 (from the assembly's peripheral row being the nearest to the core center) and No. 5 (from the assembly's peripheral row being the farthest from the core center) with the Melt B claddings manufactured with a heat-up to 1180 °C, with respectively the greatest and the smallest diameter change (Table 3).

Metallographic tests were conducted on the cladding cross-sections using a remote metallographic microscope in conditions of a safety chamber. Some of the tests were performed in laboratory conditions. The structure was identified by electroetching technique in a 10% aqueous solution of oxalic acid. Such etching is well in identifying the grain boundaries and the carbide phase in stainless steels in the region of elevated operating temperatures (Kinev 2019).

To prepare specimens for the transmission electron microscopy (TEM), a cladding piece of 3.5×3.5 mm was cut out by electrospark technique, thinned on both sides to a thickness of 0.1 mm using fine-graded grit cloth, and then spray-polished to the required thickness. Procedures based on a dark-field image in the phase reflex were used for the phase identification. The interplane distances and the angles between these obtained based on electron diffraction patterns were compared with those tabulated for the anticipated phases.

Mechanical tests of circular specimens were conducted at 600 °C with the active grip traveling rate of 1 mm/min. The performance was determined graphically using a recorded tensile diagram.

The density was determined by hydrostatic weighing of 30 mm long cladding specimens (GOST 9553-2017)

Table 1. Chemical composition of ChS-68 steel, wt. %.

C	Mn	Si	S	P	Cr	Ni	Mo	Ti	V	Al	B	N	Co
Requirements of Specs 14-131-960-2001 (Spitsyn et al. 2015)													
0.05–0.08	1.3–2	0.5–0.8	≤ 0.012	≤ 0.02	15.5–17	14–15.5	1.9–2.5	0.2–0.5	0.1–0.3	≤ 0.1	0.003–0.006	≤ 0.02	≤ 0.02
Specific concentration ratio of melting A elements to melting B elements													
1	1	0.8	0.6	0.7	1	1	0.9	1	0.8	1	0.3	1.6	0.8

Table 2. Average values of the maximum diameter changes, characteristic temperatures and irradiation doses.

Manufacturing technology	Standard technology	Heating to 1060 °C	Heating to 1180 °C
Diameter increment, %	1.36	1.0	1.02
$T_{char.}$, °C	489	481	475
$D_{char.}$, dpa	61.9	61.5	60.2

Table 3. Characteristics of tested fuel rods.

Fuel rod No.	Manufacturing technology	Diameter change, %	Irradiation parameters			
			$T_{char.}$, °C	$T_{max.}$, °C	$D_{char.}$, dpa	$D_{max.}$, dpa
1	Standard	1.9	505	583	68.4	68.6
2	Standard	1	465	623	54.5	62.8
3	Add. 1060 °C	1	470	620	55.9	62.1
4	Add. 1180 °C	1.4	470	590	63	69.4
5	Add. 1180 °C	0.9	465	571	55.7	59.4

cleaned of fuel residues mechanically and chemically. The initial density was determined by averaging the experimental density values for a series of specimens of each cladding cut out of the gas space portion not experiencing swelling. The relative density change has a physical meaning of volumetric irradiation-induced swelling.

3. Test results

Irradiation temperatures and damaging doses were calculated for the cross-sections with the maximum diameter increase. The obtained values averaged for each fuel rod group are given in Table 2 from which it can be seen that the additionally heated-up claddings have a practically similar mean relative diameter change, this being much less than for the claddings manufactured using the standard technology. And the characteristic temperatures and doses within the maximum form change (swelling) zones of the claddings heated up to 1180 °C are lower than for those heated up to 1060 °C or standard claddings.

Table 3 presents the characteristics and the form change values of the selected fuel rods. The largest and the smallest diameter change values for the claddings with the standard manufacturing technology differ by 1.9 times with the maximum dose differing by 6 dpa, as the diameter change difference for the claddings heated up additionally to 1180 °C is 1.5 times (the maximum dose difference is 10 dpa). The form change of the cladding heated up to 1060 °C is at the level of the best standard cladding with the maximum dose being ~62 dpa. The dispersion of all of the treatment technologies in the total fuel assembly mass turned out to be larger though it decreased to a certain extent in the additionally heated-up claddings.

The volumetric swelling and the swelling rates, calculated based on the characteristic doses shown in Table 3 for the claddings of fuel rods Nos. 1 and 4 with the maximum damaging doses, are noticeably higher than for the others (Table 4). The dependence of swelling on dose was assumed to be linear and no presence of the swelling incubation period was taken into account in the swelling rate calculations. The swelling rate minimum was recorded for fuel rod No. 3 with the maximum irradiation parameters being higher than for fuel rod No. 5.

The mechanical properties at 600 °C proved to be as unsatisfactory as they could be in the claddings treated using the standard technology (see Table 4). The additionally heated-up claddings showed a much higher tensile

strength (TS) and a noticeable residual ductility (d_{tot}), the positive influence on the suppression of the high-temperature irradiation embrittlement (HTIE) effect for both additional heat-up temperature modes having been identical.

The steel structure and the nature of the high-temperature physicochemical interaction of the contents within the fuel rod with the cladding, observed in the reflected light metallographic microscope, are shown in Fig. 1. Loose layers of interaction products, as in the event of continuous corrosion, occur on the inner surface of fuel rod No. 1 in the process of standard treatment and below 580 °C (Fig. 1b). As the irradiation temperature increases (Fig. 1d), as well as for the test assemblies, spots of local penetration along the grain boundaries occur at 540–595 °C against the background of continuous corrosion as it takes place during intergranular corrosion (IGC). The occurrence of the IGC spots on the claddings of all fuel rods coincides with the carbide phase precipitation on the steel grain boundaries. The exception is the fine-grained cladding of fuel rod No. 1 in which no IGC spots were detected despite the presence of carbide precipitates (Fig. 1a).

The maximum corrosion depth values recorded at the fuel rod's upper portions at the above irradiation temperature are shown in the two closing columns of Table 4. There is a deeper damage to the claddings of fuel rods Nos. 2 and 3 at 595 °C, and there is a much smaller damage to the claddings of fuel rods Nos. 4 and 5 at lower temperatures. The same pairs of rods show the most noticeably different morphology of the grain-boundary carbide precipitates. The largest adjacent carbide particles forming the grain-boundary networks precipitate in the claddings of fuel rods Nos. 2 and 3. Fuel rod No. 1 has the carbide phase morphology differing from that of the other rods, its particles being nearly uniformly distributed in the metal due to an abnormally fine grain corresponding to size 11 of the standard scale. The grain size in the claddings of all other rods corresponds to size 8 or 9 except the zone with a temperature of 570 °C near the cladding of fuel rod No. 4 which has its grain increased to size 6 or 7 and the carbide precipitates look like thin solid braids (Fig. 1g, h).

A TEM-based study of the porosity and the secondary phase precipitates has shown the following. There are a great number of pores and *G*-phase precipitates with the sizes comparable with those of the pores observed in all claddings at an irradiation temperature of 420 °C (at which the swelling reaches 70 to 80% of the maximum value). And the pore distribution in the metal of the cladding with the standard pore treatment technology is more homogeneous than in the others. The non-homogeneity in the pore distribution is expressed in the presence of pore-free zones near the grain boundaries and in the region of the twins resulting from the prior cold deformation of the initial claddings (Fig. 2). Rare precipitates of dispersed carbides ($M_{23}C_6$) are encountered along the grain boundaries and there are less such precipitates in the claddings heated up to 1180 °C, that is, there are more pore-free zones and

Table 4. Results of the irradiation influence on the cladding properties.

Fuel rod No.	Swelling, %	Swelling rate	Mechanical properties at 600 °C			Corrosion depth	
			% / dpa	TS, MPa	δ_{tot} , %	μm	T_{irr} , °C
1	4	0.058	210	0	20	575	
2	2.2	0.04	120	0	47	595	
3	2	0.036	620	1.5–2	35	595	
4	3.5	0.056	600	1.5–2	25	570	
5	2.1	0.038	650	2–2.5	15	540	

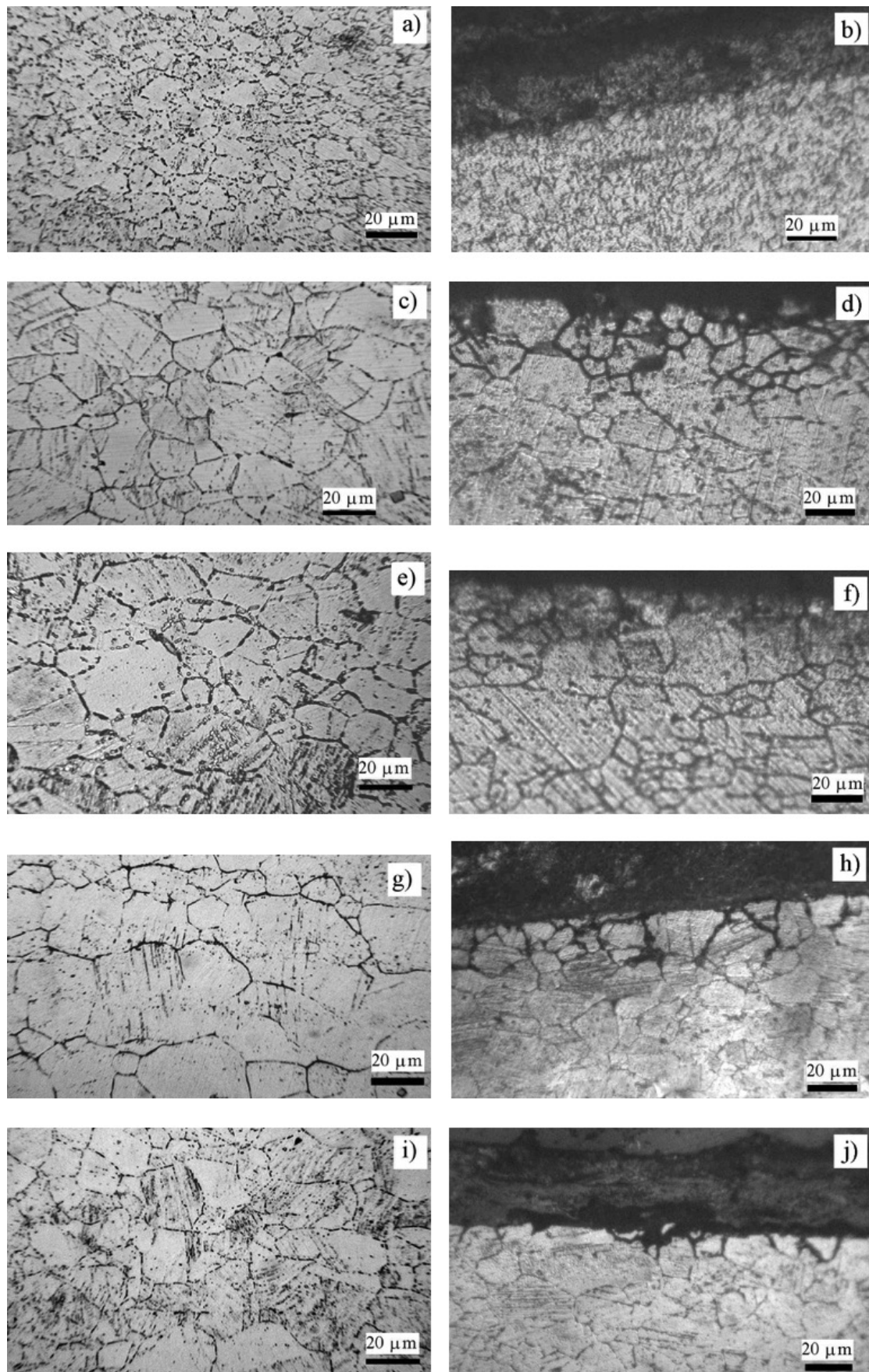


Figure 1. Cladding inner surface structure and damage: a), b) – fuel rod No. 1 (standard technology) $T_{irr.} = 575$ °C; c), d) – fuel rod No. 2 (standard technology) $T_{irr.} = 595$ °C; e), f) – fuel rod No. 3 (heated up to 1060 °C) $T_{irr.} = 595$ °C; g), h) – fuel rod No. 4 (heated up to 1180 °C) $T_{irr.} = 570$ °C; i), j) – fuel rod No. 5 (heated up to 1180 °C) $T_{irr.} = 540$ °C.

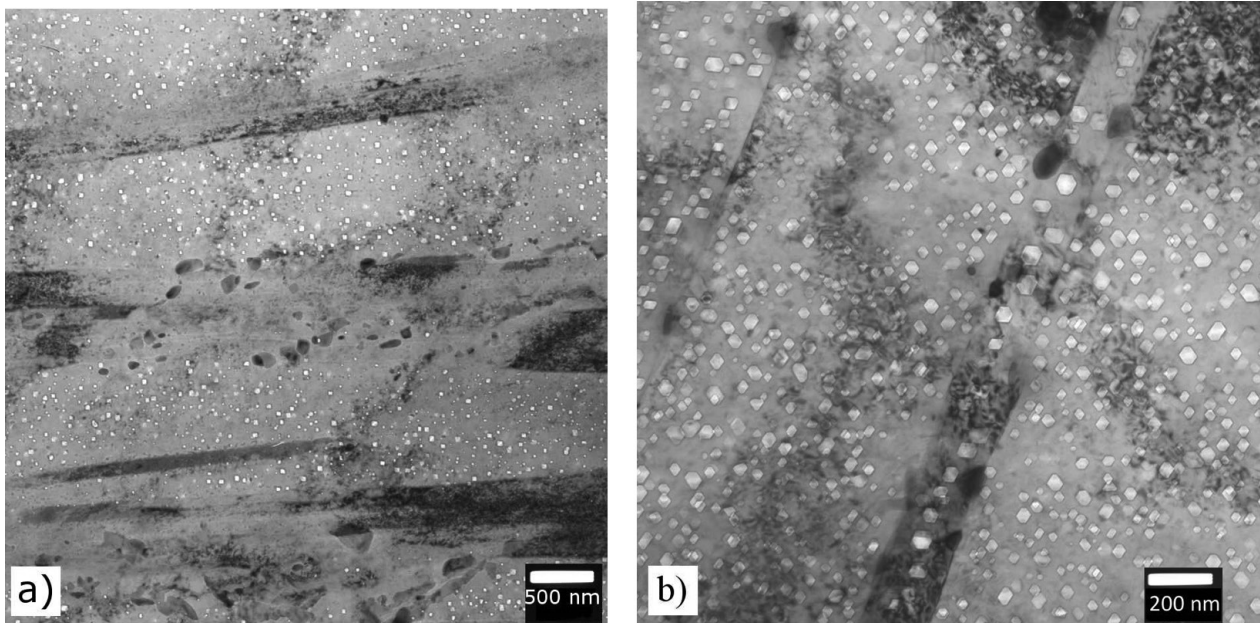


Figure 2. Nonuniform pore distribution in additionally heated-up claddings (a) and uniform pore distribution in claddings with standard technology (b).

less grain-boundary carbide precipitates in the additionally heated-up claddings at 420 °C.

The configuration of the pores and the G -phase precipitates in the zone with the maximum swelling at a temperature of about 470 °C remains approximately the same as described above, but the morphology of the grain-boundary carbide phase changes. The $M_{23}C_6$ phase precipitates become large and grow in number, while chains of adjoining precipitates form on some boundary lengths. A part of the carbides is identified as carbides of the M_6C type. More than a half of all of the visible pores in all claddings have small or the smallest dimensions but the pore concentration is noticeably higher in claddings with the standard treatment technology.

4. Discussion of results

The fine grain in the cladding of fuel rod No. 1 (two or three times as fine as in the others) can be caused only by one reason, namely by underheating in the process of austenitization at the prefinished tube size stage (Gulyaev 1977). In conditions of a rapid heat-up and a short hold time, this circumstance, except the fine grain, leads to the incomplete dissolution of the carbide particles formed in the metal in an uncontrolled manner at the preliminary tube conversion stages, as well as the uncompleted recrystallization process and the associated structural non-equilibrium of the alloy (Tselishchev et al. 2006).

On the contrary, fuel rod No. 4 has its grain at the cladding top increased to size 6 or 7 and featuring “non-continuous” boundaries and a high non-homogeneity size ratio (Fig. 1g, h). These are the symptoms of the secondary recrystallization occurring by an in-situ mechanism caused

by the disappearance of weakly disoriented boundaries thanks to the grain rotation. Therefore, the steel overheating was taking place and, apparently, in the process of austenitization at the tube prefinished size stage.

Fuel rods Nos. 1 and 4 (each in its group) are the carriers of the greatest diameter changes and the largest volumetric swelling. These fuel rods have noticeably larger damaging doses, and rod No. 4 also has a higher temperature. However, when comparing the swelling of these with the swelling of fuel rods Nos. 2 and 5 manufactured using similar technologies, the nearly twofold increase in the swelling rate cannot be explained only by the “harder” irradiation conditions. The suboptimal state of the metal caused by the above process irregularities is sure to have made its own contribution the amount of which is hard to estimate based on the available data. However, the structural state analysis conducted for the claddings of fuel rods Nos. 1 and 4 can lead to a fundamental conclusion that the major reason for the decrease in the metal resistance to the reactor medium damaging factors and for the dispersion of the irradiated cladding properties are deviations in the temperature mode of austenitization at the tube prefinished size stage that were not regulated and not observed on time. Though the peculiarities of the overall conversion technology can also make a contribution of their own, both positive and negative, one cannot as well exclude in full the irradiation temperature non-uniformity in conditions of a hard-to-control coolant flow velocity around the deforming claddings.

When comparing the properties of the claddings of fuel rods Nos. 2, 3, and 5 with the experience of operation in close temperature and dose conditions, preference shall be given to the technology using which the cladding of fuel rod No. 3 was manufactured (and heated up addi-

onally to 1060 °C). The basis for this is the best combination of the properties tested for (see Table 4), as well as better workability and cost-effectiveness as compared with the claddings heated up to 1180 °C.

We shall consider the potential results of a positive effect from additional heat-ups. A heat-up to 1060 °C with a hold time of 20 min makes the carbon fixed in carbide phases of the $M_{23}C_6$ and MC types formed in the process of the tube manufacturing “metallurgical” preparation (from the ingot to the hot-forged billet) pass into austenite. In the event of a heat-up to 1180 °C with a long hold time, first, an additional amount of the carbon fixed in carbonitride will pass into the austenite, and, second, the chemical composition will equalize diffusively in the zones enriched by alloying elements tending to being liquation, primarily by molybdenum. The addition of free carbon to the austenite will be small due to a normally minor content of carbonitrides in steel, and the requirement for homogenization by molybdenum at the intermediate diameter billet stage is doubtful provided the ingot has been homogenized correctly and parts of the ingot have been correctly selected for the tube conversion.

The carbon dissolved in the austenite in the process of the cladding operation is fixed in carbides and precipitates on large-angle grain boundaries and non-coherent twin boundaries. It was observed in the process of the metallographic study that grain-boundary carbides started to occur in the claddings of fuel rods Nos. 2 and 3 at an irradiation temperature of 440 °C, and in the cladding of fuel rod 5 at a temperature of 465 °C, which is likely to be caused by the temperature of heat-up (to 1060 or 1180 °C) and by the difference in the uniformity of the carbon distribution in the austenite lattice. This is additionally evidenced by the cladding of fuel rod No. 4 assumingly heated up and, therefore, having a still higher carbonic homogeneity where the initial carbides occur at a temperature of above 465 °C. The carbide deposition on the boundary is the consequence of the manifested horophilic properties of carbon (Novikov 1986), and the earlier or the later formation of carbides depends on the length of the carbon atom diffusion path to the boundary, that is, on the homogeneity of the carbon distribution in the austenite lattice (Goldsh-teyn et al. 1985). A note shall be also made of a positive effect the controlled quantities of horophilic boron and phosphorus (Vatulin and Tselishchev 2004), the content of which in Melt B is larger than in Melt A (see Table 3), has on the morphology of carbides.

Due to the grain-boundary carbide formation and swelling maximum temperatures being close, the processes of carbide and pore formation can be logically expected to be mutually dependent. The pore formation grows in intensity with the increase in the quasi-equilibrium concentration of vacancies (Zelenskiy et al. 1988). The carbon dissolved in austenite plays supposedly the role of neutral sinks and stops to act as such as it is fixed in carbides and the number of the vacancies capable to form pores gets larger. Atoms of such alloying elements as molybdenum and silicon, which form part of M_6C -type carbides, may

have a contribution of their own to swelling. As they leave austenite and enter carbides, they also stop to act as neutral sinks and the swelling grows more intense. Such role of Mo and Si can be assumed from an analysis of the electron microscopy data for the samples irradiated at 420 °C. No carbide formation is observed at this temperature, still numerous *G*-phase particles occur as compounds with the $M_6Ni_{16}Si_7$ formula where M are atoms of Fe, Mo, Cr, Mn, and Ti. This also involves the intense formation of pores with dimensions comparable with those of the *G*-phase particles, as the swelling reaches 80% of the maximum value.

The *G*-phase formation takes place also at the characteristic temperature of the maximum swelling (470–490 °C), this being of an approximately similar intensity in claddings of all types. Simultaneously, carbides form actively at these temperatures, intensifying so the pore formation and increasing the swelling to the maximum.

The occurrence of residual ductility during ring specimen testing at 600 °C may be caused by the peculiarities of the pore distribution in the structure. With the deformation capacity of the grain body assumed to have been reduced to zero by numerous small-size pores, and the grain boundaries to have lost their strength due to the impact of neutrons, a more homogeneous arrangement of pores within the grain body will lead to a more pronounced embrittlement with the intergranular type of failure, exactly what is observed in the cladding with the standard manufacturing technology (No. 2). The grain body in claddings with another technology retains, in the process of irradiation, more structure areas free of pores and with the capacity for plastic strain acts, this causing the irradiated metal to keep some of its ductility.

It is observed that the depth of the IGC-type cladding damage inside of the fuel rod correlates with the morphology of the grain-boundary carbides. A deeper disintegration of the grain boundaries in the surface layers of the metal takes place in the event that there are carbide networks of adjoining carbide particles present on the boundaries, as it is the case in the cladding of fuel rod No. 2 with the standard manufacturing technology. Special attention shall be given to the negative effect the grain growth has on the corrosion depth.

The technology of tube manufacturing from Melt A uses rapid heat-up with a short hold time. This is likely what leads exactly to a differently non-equilibrium state of the structure, including the incomplete passing of fixed carbon into austenite, a less uniform distribution of free carbon, and, potentially, preservation of zones with the chemical composition close to that of carbides, a sort of “pre-precipitates”. Pre-precipitates may have the role of substrates that accelerate the irradiation-induced precipitation of carbides, and intensify therefore the pore formation. Pre-precipitates are most likely to exist in claddings with the standard technology and, as a matter of fact, the concentration of pores in the cladding of fuel rod No. 1 in the maximum swelling zone is one time and a half as high as in the other claddings.

The technology of tube manufacturing from Melt B with a heat-up that provides for a more complete dissolution of carbon-containing phases is not likely to require at all the heat-up to 1060 or 1180 °C at the billet intermediate diameter stage. Still, a reduction in the dispersion of properties evidently requires thorough individual austenitization of each cladding at the prefinished size stage with the strictly controlled temperature mode and hold time.

5. Conclusion

1. The major reason for the dispersion in the properties of spent fuel claddings is the initial cladding heterogeneity in terms of the content of carbon which is partially dissolved in austenite and is present in part in

the state of carbide “pre-precipitates”. Irradiation-induced formation of carbides takes place at different temperatures and has different intensity, having so an accelerating effect on swelling and corrosion.

2. The uncontrolled carbon heterogeneity of metal results both from the ingot manufacturing process and the metal hot treatment for the initial billet fabrication and from the process of tube conversion (recrystallization annealing and austenitization at the prefinished size stage).
3. An improvement of the tube technology will lead unambiguously to a more favorable condition of the initial claddings in terms of carbon content, regarding the irradiation-induced swelling, still the pattern used for the austenitizing heat-up at the prefinished size stage retains a great deal of variations for the initial tube condition.

References

- Bakanov MV, Chuev VV, Kryukov OV, Lukin AV, Bychkov SA, Budanov YuP, Korostin OS, Tselishchev AV, Tarasyuk VB (2005) Optimization of the structural state of the ChS-68 steel cladding tubes in a cold-worked condition. *Izvestiya Vysshikh Uchebnykh Zavedeniy. Yadernaya Energetika 1*: 139–145. [in Russian]
- Bakanov MV, Maltsev VV, Oshkanov NN, Chuev VV (2011) Key results of the operation of structural materials in the BN-600 reactor cores. *Izvestiya Vysshikh Uchebnykh Zavedeniy. Yadernaya Energetika 1*: 177–186. [in Russian]
- Bakanov MV, Maltsev VV, Oshkanov NN, Chuev VV (2011a) Key results of the performance testing of fuel rods with new-generation austenitic steel claddings. *Izvestiya Vysshikh Uchebnykh Zavedeniy. Yadernaya Energetika 1*: 187–195. [in Russian]
- Barsanova SV, Kozlov AV, Shilo OB (2018) Influence of fast neutron irradiation on the change in the mechanical properties of the EK-164 and ChS-68 austenitic steels. *VANT. Ser. Materialovedeniye i novye materialy 1(96)*: 4–12. [in Russian]
- Goldshteyn MI, Grachev SV, Veksler YuG (1985) *Special Steels*. Metallurgiya Publ., Moscow, 408 pp. [in Russian]
- GOST 9553-2017 (2018) *Glass and Glassware. Density Determination Technique*. Moscow, Izdatelstvo Standartov Publ. [in Russian]
- Gulyaev AP (1977) *Material Science*. Metallurgiya Publ., Moscow, 646 pp. [in Russian]
- Kinev YeA (2019) Correlation of high-dose radiation swelling of the 16Cr – 15Ni steel class with the grain size. *Perspektivnye materialy 3*: 39–46. [in Russian]
- Novikov II (1986) *The Theory of Metal Thermal Treatment*. Metallurgiya Publ., Moscow, 480 pp. [in Russian]
- Portnykh IA, Glushkova NV, Panchenko VL, Kinev YeA, Kozlov AV (2007) Differences in the irradiation-reduced swelling of ChS-68 steel fuel claddings under close neutron irradiation conditions. *VANT. Ser. Materialovedeniye i novye materialy 1(68–69)*: 377–388. [in Russian]
- Spitsyn YeV, Tselishchev AV, Budanov YuP (2015) A study into the influence of austenitic heating modes on the structural state and the endurance and creep characteristics of the ChS68-ID steel fuel rod tubes. *VANT. Ser. Materialovedeniye i novye materialy 2(81)*: 4–14. [in Russian]
- Tselishchev AV, Ageev VS, Budanov YuP, Ioltukhovskiy AG, Mitrofanova NM, Leontyeva-Smirnova MV, Shkabura IA, Zabudko LM, Kozlov AV, Maltsev VV, Povstyanko AV (2010) Development of a structural steel for fuel rods and FAs of fast sodium reactors. *Atomnaya Energiya 108(4)*: 217–222. [in Russian]
- Tselishchev AV, Ageev VS, Budanov YuP, Mitrofanova NM, Novikov VV (2006) Development and application of a microstructural approach for the development of radiation-resistant austenitic steels. *VANT. Ser. Materialovedeniye i novye materialy 1(66)*: 304–312. [in Russian] <https://doi.org/10.1007/s10512-010-9289-9>
- Vatulin AV, Tselishchev AV (2004) Structural steels for the fast neutron reactor cores. *Materialovedeniye i Termicheskaya Obrabotka Metallov 11*: 13–18. [in Russian] <https://doi.org/10.1007/s11041-005-0003-9>
- Zelenskiy VF, Neklyudov IM, Chernyaeva TP (1988) *Radiation-induced Defects and Swelling of Metals*. Naukova dumka Publ., Kiev, 296 pp. [in Russian]